Spatial correlation of OH Meinel and O_2 Infrared Atmospheric nightglow emissions observed with VIRTIS-M on board Venus Express

J.-C. Gérard[a], L. Soret[a]

G. Piccioni[b] and P. Drossart[c]

[a]Laboratoire de Physique Atmosphérique et Planétaire, Université de Liège, B-4000 Liège, Belgium, jc.gerard@ulg.ac.be, lauriane.soret@ulg.ac.be

[b]IASF-INAF, Via Fosso del Cavaliere, 100, 00133 Rome, Italy, giuseppe.piccioni@iasf-roma.inaf.it

[c]LESIA, Observatoire de Paris, 92190, Meudon, France, pierre.drossart@obspm.fr

Corresponding author:

J.-C. Gérard, LPAP, Université de Liège, 17 allée du 6 août, B5c, B-4000 LIEGE (Belgium), E-mail: jc.gerard@ulg.ac.be, Phone: +32-4-3669775, Fax: +32-4-3669711

Running title: Spatial correlation of OH and O_2 nightglow on Venus

August 2011

ABSTRACT

We present the two-dimensional distribution of the O_2 $a^1\Delta$-$X^3\Sigma$ (0-0) band at 1.27 µm and the OH Δv=1 Meinel airglow measured simultaneously with the Visible and Infrared Thermal Imaging Spectrometer (VIRTIS) on board Venus Express. We show that the two emissions present very similar spatial structures. A cross-correlation analysis indicates that the highest level of correlation is reached with only very small relative shifts of the pairs of images. In spite of the strong spatial correlation between the morphology of the bright spots in the two emissions, we also show that their relative intensity is not constant, in agreement with earlier statistical studies of their limb profiles. We conclude that the two emissions have a common precursor that controls the production of both excited species. We argue that atomic oxygen, which produces $O_2(^1\Delta)$ molecules by three-body recombination and is the precursor of ozone formation, also governs to a large extent the OH airglow morphology through the $H + O_3 \rightarrow OH^* + O_2$ reaction.

Keywords: Venus, atmosphere, aeronomy, composition

I. INTRODUCTION

The OH (2-0) band near 1.45 μm, the (1-0), (2-1) and possibly (3-2) Meinel bands near 3 μm were discovered by Piccioni et al. (2008) in limb spectra obtained with the Visible and Infrared Thermal Imaging Spectrometer (VIRTIS) on board Venus Express. They indicated that the limb intensities are 880 ± 90 kiloRayleighs (1 Rayleigh = 10^6 ph.cm^{-2} s^{-1} in 4π st) for the (Δv=1) sequence and 100 ± 40 kR for OH (Δv=2). The intensity measured along the line of sight peaked at an altitude of 96 ± 2 km near midnight, in the case of the orbit used for the analysis. Taking these characteristics into account and assuming a conversion factor of 55.4 between limb and the vertical observations, the associated vertical emission rates were estimated at 16 kR and 1.8 kR, respectively. These emission rates are 55 ± 5 and 480 ± 200 times weaker than the bright O_2 ($a^1\Delta$) (0-0) band intensity at 1.27 μm (Piccioni et al., 2008). For a total of 10 orbits examined, the peak altitude appeared to remain constant within the vertical resolution of the measurements. The OH (1-0) P1(4.5) and (2-1) Q1(1.5) OH airglow lines were recently detected by Krasnopolsky (2010) using a ground-based telescope. The total hydroxyl emission rate derived from these observations was consistent with the value obtained by Piccioni et al. (2008). Gérard et al. (2010) analyzed a larger set of VIRTIS limb images and found that the intensity of both emissions reach their larger statistical intensity in the region of the anti-solar point and is dimmer in the vicinity of the terminator. The average altitude of the OH limb emission they derived from the limb images was 95.3 ± 3 km for OH(Δv=1). The brightness of the peak intensities of the O_2 ($a^1\Delta$) and OH Meinel emissions shows some degree of correlation. They suggested that the global subsolar to antisolar circulation plays a key in the control of both airglow emissions. Recently, Soret et al. (2010) analyzed the full set of 3328 VIRTIS-M limb profiles of the OH nightglow. They showed that the emission is highly variable and that the mean peak intensity along the line of sight of the OH $\Delta v = 1$ sequence is located at 96.4 ± 5 km. The peak brightness appears to decrease from the antisolar point, but the variability at any given location is very strong. They also found that the intensity of the OH and O_2 (a $^1\Delta$) peak emissions are correlated, although the ratio between the two emissions shows a great deal of variability.

By contrast, the O_2 $a^1\Delta$ - $X^3\Sigma$ (0-0) band emission at 1.27 μm, the strongest Venus nightglow emission, was first observed more than 30 years ago by Connes et al. (1979) using Fourier transform spectroscopy from the ground. Subsequent spatially resolved ground-based observations (Allen et al., 1992; Crisp et al., 1996; Lellouch et al., 1997; Ohtsuki et al., 2008; Bailey et al., 2008a,b) have demonstrated that the spatial distribution of the O_2 ($a^1\Delta$) infrared airglow is quite variable in space and time. Nightside images indicate that these rapidly changing bright areas occur most frequently at low latitudes between midnight and 03:00 local time. During the Venus flyby by Galileo, Drossart et al. (1993) observed with the Near-Infrared Mapping Spectrometer (NIMS) a large enhancement of the 1.27 μm emission near 40°S, over a spatial area ~100 km wide. The apparent motion of gas masses transported by horizontal winds has been analyzed by Hueso et al. (2008) using the O_2 (a-X) airglow. This study showed that the details of the distribution changed over 30 min, but indicated that large structures usually persist over several hours.

Drossart et al. (2007a) determined from VIRTIS-M limb observations that the O_2 ($a^1\Delta$) peak emission is located near 96 km, an altitude which is consistent with excitation by three-body recombination of oxygen atoms as proposed by Connes et al. (1979). Gérard et al. (2008) analyzed the distribution of the O_2 ($a^1\Delta$) infrared nightglow observed with VIRTIS-M. They presented a first statistical map of the average in the southern hemisphere observed with VIRTIS over an 11-month period of low solar activity. They found that the distribution is characterized by an enhanced brightness region located near the midnight meridian at low latitude. The location of the bright airglow region was further studied by Piccioni et al. (2009) who confirmed that it is centered on the anti-solar point. Soret et al. (2011) obtained statistical distributions of the airglow profiles for different sets of solar zenith angles. They showed that the altitude of the O_2 airglow peak tends to increase by about two kilometers between the terminator and the antisolar point. They combined limb and nadir observations from the VIRTIS instrument to generate a three-dimensional map of the O_2 ($a^1\Delta$) emission in the mesosphere-thermosphere transition region on the Venus nightside from which they derived the global distribution of atomic oxygen on the nightside. They obtained a mean vertical brightness of 0.50 MR, quite close to the 0.52 MR derived by Piccioni et al. (2009) and 0.55 MR by Krasnopolsky (2010). Piccioni et al. (2009) obtained a statistical mean value of 97.4 ± 2.5 km for the peak altitude of the volume emission rate, in close agreement with the 96 ± 2.7 km determined by Gérard et al. (2010) for the maximum intensity along the line of sight. They showed that the vertical profile is broader near the equator, with a full width at half maximum of 11 km, a factor of 2 larger than at middle latitudes. Migliorini et al. (2011) showed that the limb profiles of the different OH spectral bands have a very similar altitude dependence.

Gérard et al. (2009) analyzed simultaneous nadir observations of ultraviolet nitric oxide nightglow made with the Spectroscopy for Investigation of Characteristics of the Atmosphere of Venus (SPICAV) instrument and O_2 ($a^1\Delta$) emission with VIRTIS-M. Unexpectedly, they found that the two emissions are frequently spatially uncorrelated, showing little resemblance. This difference in the spatial distribution of the O_2 and NO emissions was interpreted as an indication of the presence of horizontal winds carrying the long-lived oxygen atoms during the 15-20 km descent separating the nitric oxide from the O_2 airglow layer. The efficiency of horizontal winds to delocalize regions of enhanced brightness in the two emissions was demonstrated by Collet et al. (2011) with a chemical-transport two-dimensional model. We use VIRTIS limb images to analyze and quantify the spatial correlation between the O_2 ($a^1\Delta$) and the OH Meinel IR nightglow emissions. In this study we show that, by contrast to the lack of spatial correlation between NO and O_2 ($a^1\Delta$) airglows, the O_2 and OH emissions show a high degree of spatial correlation in the 90-110 km region. We discuss the processes potentially explaining this result in the light of recent observation of ozone in the nightside lower thermosphere of Venus.

II. OBSERVATIONS

Following final orbital insertion, the Venus Express spacecraft was on an elliptical orbit with a period of 24 hours, an apocenter at 66,000 km and a pericenter at 250 km, located at 80° N (*Svedhem et al*., 2007; *Titov et al*., 2006). It is fixed in inertial space so that it precesses in local time by about 6.4 min/24 hours. The VIRTIS instrument and its operating modes have been described by *Drossart et al*. (2007a) and *Piccioni et al.* (2008). It consists of two spectrometers (Piccioni et al., 2009): VIRTIS-M devoted to spectral mapping, and VIRTIS-H a high-resolution spectrometer. VIRTIS-M utilizes two different detectors, a silicon charge coupled device for the visible channel covering the 0.25-1μm wavelength range and a HgCdTe infrared focal plane array for the infrared channel covering the 1-5 μm wavelength range. In brief, the VIRTIS-M infrared channel provides spectral cubes at a spectral resolution R~200. The spectral sampling is ~10 nm throughout the spectral range of the instrument . A spatial scan, covering a 64 mrad x 64 mrad field of view, is obtained using a scanning mirror or push-broom technique. VIRTIS-M therefore progressively builds up two-dimensional images for each of the 432 spectral bands. The 0.25 mrad pixel size of the VIRTIS-M detector projected on Venus limb provides a spatial resolution of 1.9 km for a spacecraft distance of 7500 km, a value which is typical of a VIRTIS observation at 40° N. For 8-s exposures, the acquisition time of a full 256 × 256 pixel image takes about 50 min. The absolute pointing accuracy is typically better than ±1/7th of a pixel (Piccioni et al., 2009).

A total of 1356 limb images have been obtained, covering a period extending from 15 May 2006 to October 14 2008. For each limb observation, all intensities of pixels with identical latitudes and local times but different altitudes have been grouped together to ultimately obtain an intensity profile as a function of the altitude of the minimum ray height. O_2 and OH (Δv=1) vertical profiles averaged over bins of 3° of latitude x 0.5 km of altitude have been extracted in this way from the limb images. Analysis of the spectral cubes in the vicinity of 1.27 µm at the limb indicates that the thermal radiation from the lower atmosphere is very small for altitudes of the tangent point above ~85 km and thermal background corrections are negligible above 90 km (Piccioni et al., 2008b). However a contribution, presumably caused by scattering of thermal emission by haze, has to be removed from the raw profile in the region of the much weaker OH emission. The methodology described by Soret et al. (2011) to remove this contribution has been applied. A third order polynomial fit was determined to represent the thermal emission above 110 km. The same procedure was applied to fit the thermal emission below 85 km. The two polynomial fits have been subsequently smoothly connected. Adjacent latitudinal bins were assembled to create maps of the limb brightness distribution of the two emissions between 90 and 110 km. Following application of this thermal background subtraction, a number of images showed a low S/N ratio for the OH signal with an OH peak intensity too weak to be distinguished from thermal contribution. For this analysis, a selection has been made to only keep those profiles exhibiting a discernable emission peak. Using the 1356 limb profiles obtained this way, 94 images have been generated. Finally, following visual inspection, a subset of 93 simultaneous O_2 and OH airglow images were selected. Finally, only the 32 images covering a latitudinal extent larger than 5° were used for the spatial correlation analysis.

III. OH (Δv=1) AND O_2 ($a^1\Delta$) AIRGLOW LIMB IMAGES

Figure 1 shows examples of the limb intensity distribution of the O_2 ($a^1\Delta$) and OH $\Delta v=1$ emissions measured simultaneously with VIRTIS-M. In each of these examples, the local time of the observations varies by less than 3 hours as a consequence of the high inclination of the Venus Express orbit. Therefore, these intensity maps may, in the first order, be considered as latitudinal cuts at a nearly fixed local time. For example, in panel 1-a (orbit 733, 23 April 2008) the latitude coverage extends from 4° to 31° N. The data were obtained over a total observing time of 61 minutes and these distributions may be considered as snapshots of the intensity between 23:02 and 01:43 local time. They reveal a striking resemblance between the spatial (latitude, altitude) distributions of the two emissions. In Figure 1-a1, a bright region of 1.27 µm emission reaching ~140 MR is seen in limb view at 95 km near 27°, with a corresponding enhanced OH spot with a maximum brightness of ~ 1 MR. The detailed spatial structures of the two emissions are very similar and the OH emission peaks at the same altitude as O_2 1.27 µm. A second region of enhanced airglow, less pronounced than the first one, is observed in both emissions near 9°. Although the OH observation is more noisy, the structure of this secondary emission and the region of less intense emission near 18° are again very similar. Panels (b), (c) and to a lesser extent (d) illustrate other examples of meridional distributions of the two airglow emissions. They were selected because they cover a reasonably wide range of latitudes in the northern hemisphere and visually illustrate the similar distributions observed in the database. Panel (b) illustrates an additional characteristic of the spatial correlation. In this example (orbit 499, 2 September 2007), two bright spots are observed in both emissions. The altitude of the airglow drops with increasing latitude by ~4 km over a 12° latitude span. The same change is observed in the altitude of the OH emission peak. In both cases, the higher latitude bright spot is likely associated with stronger vertical transport carrying the atoms and the airglow layers to a lower altitude than in the other region of enhanced emission. Panel (c) shows a reversed situation. In this case, the bright spot near 55° is at an altitude approximately 4 km higher than the other enhanced region for both emissions. A suggestion of the third slightly enhanced region is also observed near the southern edge of the VIRTIS image. The fourth case illustrated in panel (d) also reveals several regions of enhanced O_2 ($a^1\Delta$) emission and a drop of the peak altitude between 55° and 72°. However, in this case, only a weak enhancement of OH emission is associated with the bright O_2 spot located at 103 km near 51°N. This is the only case in the database when no obvious morphological correlation is seen between the two emissions. It clearly illustrates that the intensity ratio of the O_2 and OH airglow is variable, a point that will be discussed in further details in section IV.

We now quantitatively examine the degree of spatial correlation between the two emissions. For this purpose, we calculate the cross correlation matrix between the 32 simultaneous images mentioned in section II, except that they have been re-dimensioned so that only pixels with a positive value are considered. Assuming that those two (O_2 and OH) spectral images have a common dimension I x J, for each set of two images, the $R(i,j)$ elements of the correlation matrix of dimensions I x J are calculated as:

$$R(i,j) = \frac{\sum_x \sum_y \left[f_1(x,y) - \overline{f_1(x,y)}\right] \times \left[f_2(x-i,y-j) - \overline{f_2(x,y)}\right]}{\left[\sum_x \sum_y \left[f_1(x,y) - \overline{f_1(x,y)}\right]^2 \times \sum_x \sum_y \left[f_2(x-i,y-j) - \overline{f_2(x,y)}\right]^2\right]^{\frac{1}{2}}}$$

with i = 0, 1, 2, …, I and j = 0, 1, 2, …, J

where $\overline{f_1}$ is the average value of $f_1(x,y)$ which represents the intensity matrix in the O_2 limb image and $\overline{f_2}$ is the average value of $f_2(x,y)$ which is the intensity matrix of the OH image. Near the edges, only pixels with positive value are considered. The $R(i,j)$ matrix elements vary between -1 and 1, independent of the intensity scale of the two emissions. The maximum value of $R(i,j)$ determines the shift in altitude or latitude that optimizes the correlation between the two images.

The results of this cross-correlation study confirm the high degree of correlation suggested by the examples in Figure 1. For examples, the maximum correlation coefficients and the associated shift for the OH images with respect to the O_2 images for the cases shown in panels (a), (b), (c) and (d) are 0.91 (-1°, 0.5 km), 0.88 (+2°, -0.5 km), 0.92 (0°, 0.5 km) and 0.77 (0°, 0.5 km) respectively. If the whole set of 32 couples of images is used, the mean correlation coefficient is 0.81 with mean displacements of -0.1° and 0.4 km. The extreme values of the altitude shift are only -0.5 and +1 km. These results show that the two emissions have a very similar peak altitude and latitude. The similar altitude distribution of OH and O_2 had been noticed by Piccioni et al. (2008), Gérard et al. (2010), Migliorini et al. (2010) and Soret et al. (2010).

As mentioned before, the relationship between the intensity of the OH airglow at the peak versus that of O_2 shows a large degree of scatter as was illustrated in Figure 4 by Soret et al. (2010). This may appear in conflict with the results presented here which demonstrate a high level of spatial correlation. To investigate this apparent paradox, we have determined the maximum intensity of both emissions for each bright spot such as described in Figure 1. Specifically, a 5x5 pixel square, corresponding to 5° of latitude x 2.5 km of altitude of the tangent point, has been centered on the brightest pixel of each bright region of O_2 ($a^1\Delta$) airglow. The average brightness has been determined and compared to the corresponding region in the OH emission, eventually shifted by the amount of pixels determined from the cross-correlation analysis. The resulting plot is shown in Figure 2 together with the linear least-squares fit regression. The correlation coefficient R=0.52 and the slope is 4.4×10^{-3}. These values are comparable with those obtained by Soret et al. (2010) who used 1356 vertical limb profiles and found R= 0.47 and a regression slope of $5.5 \times 10^{-3.}$ We thus conclude that the scatter previously observed is consistent with this analysis: the clear spatial correlation is compatible with a variable ratio of the brightness of the two emissions.

IV DISCUSSION

The results presented in this study clearly demonstrate that the O_2 ($a^1\Delta$) and the OH Meinel airglow emissions on the Venus nightside are closely linked by a common precursor controlling their horizontal and vertical distribution to a large extent. Earlier studies (Piccioni et al., 2008; Soret et al., 2010) have proposed that the link between the two emissions is atomic oxygen which is the direct source of O_2 ($a^1\Delta$) molecules through the three-body process:

$$O + O + M \rightarrow O_2\,(a^1\Delta) + M$$

and the precursor of ozone:

$$O + O_2 + M \rightarrow O_3 + M$$

which reacts with atomic hydrogen to produce excite hydroxyl radicals:

$$O_3 + H \rightarrow OH\,(v < 10) + O_2$$

The presence of an ozone layer near 100 km on the Venus nightside was recently discovered by Montmessin et al. (2011) through its absorption in the Hartley continuum using the stellar occultation technique with the SPICAV instrument. The observations indicate that the O_3 spectral signature is frequently undetected, implying that the column density at the limb is below the detection threshold near 10^{15} cm^{-2}. When observed, the ozone density is between 1×10^7 and 1×10^8 cm^{-3}, but shows a great deal of spatial variability, suggesting a patchy structure. We interpret the presence of bright O_2 and OH airglow spots as the signature of regions with enhanced O density caused by spatially varying transport efficiency. According to the nightside model by Krasnopolsky (2010), the vertical distribution of hydrogen is expected to be quite flat and to vary by less than a factor of two between 92 and 119 km. If the H distribution is relatively homogeneous, then the O density distribution marks its imprint directly on the O_2 airglow through reaction (1) and indirectly on the OH emission through reaction (2) which controls the ozone production rate. The key role of atomic oxygen probably explains the high level of spatial correlation between the intensity of the two emission features.However, the O2 airglow also depends on the density of the third body (essentially CO2), whereas the OH is proportional to the H density. Local variations of the H/CO2 ratio in the nightside lower thermosphere therefore possibly account for the observed scatter and outlying data points from a linear regression in Figure 2. Future three-dimensional modeling should help clarify this question and validate this concept.

Acknowledgments. We gratefully thank all members of the ESA Venus Express project and of the VIRTIS scientific and technical teams. L. Soret was supported by the PRODEX program managed by the European Space Agency with the help of the Belgian Federal Space Science Policy Office. J.C.G. acknowledges funding from the Belgian Fund for Scientific Research (FNRS). This work was also funded by Agenzia Spaziale Italiana and the Centre National d'Etudes Spatiales.

References

Allen, D., D. Crisp, and V. Meadows (1992), Variable oxygen airglow on Venus as a probe of atmospheric dynamics, Nature, 359, 516-519.

Bailey, J., V.S. Meadows, S. Chamberlain, and D. Crisp (2008). The temperature of the Venus mesosphere from O_2 ($a^1\Delta_g$) airglow observations, Icarus, 197, 247, doi: 10.1016/j.icarus.2008.04.007.

Crisp, D., V.S. Meadows, B. Bézard, C. de Bergh, J.P. Maillard, and F.P. Mills (1996). Ground based near-infrared observations of the Venus nightside: 1.27 μm $O_2(^1\Delta_g)$ airglow from the upper atmosphere, *J. Geophys. Res*., 101, 4577-4594.

A. Collet, C. Cox, J.-C. Gérard (2010), Two-dimensional time-dependent model of the transport of minor species in the Venus night side upper atmosphere, Planet. Space Sci., 58, 1857-1867, doi: 10.1016/j.pss.2010, 08016.

Connes, P. Noxon, J. F. Traub, and W.A. Carleton (1979). O_2 $^1\Delta$ emission in the day and night airglow of Venus, *The Astrophysical Journal*, 233, L29-L32.

Drossart, P. et al. (1993). Search for spatial variations of the H_2O abundance in the lower atmosphere of Venus from NIMS-Galileo, *Planet. Space Sci*., 41, 495-504, doi:10.1016/0032-0633(93)90032-W.

Drossart, P. et al. (2007a). Infrared spectral imaging observations of Venus by VIRTIS reveal a dynamical upper atmosphere, *Nature*, *450*, doi :10.1038/nature06140.

Drossart, P., et al. (2007b), Scientific goals for the observation of Venus by VIRTIS on ESA/Venus Express mission, Planet. Space Sci., 55, 1653–1672, doi:10.1016/ j.pss.2007.01.003.

Gérard, J.-C., A. Saglam, G. Piccioni, P. Drossart, C. Cox, S. Erard, R. Hueso, and A. Sánchez-Lavega (2008), Distribution of the O_2 infrared nightglow observed with VIRTIS on board Venus Express, Geophys. Res. Lett., 35, L02207, doi:10.1029/2007GL032021.

Gérard, J.-C., C. Cox, L. Soret, A. Saglam, G. Piccioni J.-L. Bertaux and P. Drossart (2009), Concurrent observations of the ultraviolet nitric oxide and infrared O_2 nightglow emissions with Venus Express, Icarus, J. Geophys. Res., 114.

Gérard, J.-C., L. Soret, A. Saglam, G. Piccioni, and P. Drossart (2010), The distributions of the OH Meinel and $O_2(a^1\Delta$ - $X^3\Sigma)$ nightglow emissions in the Venus mesosphere based on VIRTIS observations, Adv. Space Res., 45, 1268-1275, doi:10.1016/j.asr.2010.01.022.

Hueso, R., A. Sánchez-Lavega, G. Piccioni, P. Drossart, J.-C. Gérard, I. Khatuntsev and, L. Zasova (2008), Morphology and Dynamics of Venus Oxygen Airglow, J. Geophys. Res., 113, E00B02, doi:10.1029/2008JE003081.

Krasnopolsky, V. A. (2010), Venus night airglow: ground-based detection of OH, observations of O_2 emissions, and photochemical model, Icarus, doi:10.1016/ j.icarus.2009.10.019.

Lellouch, E., Clancy, T., Crisp, D., Kliore, A., Titov, D., Bougher, S.W (1997), Monitoring of mesospheric structure and dynamics, in: Bougher, S.W., Hunten, D.M., Philips, R.J. (Eds) Venus II: Geology, Geophysics, Atmosphere, and Solar Wind Environment, The Univ. of Arizona

Press, Tucson.

Migliorini, A., G. Piccioni, A. Cardesín Moinelo, and P. Drossart (2011), Hydroxyl airglow on Venus in comparison with Earth, Planet. Space Sci., in press.

Montmessin, F., J.-L. Bertaux, F. Lefèvre, E. Marcq, D. Belyaev, J.-C. Gérard, O. Korablev, A. Fedorova, V. Sarago, and A.-C. Vandaele, A layer of ozone detected in the atmosphere of Venus, Icarus, submitted.

Ohtsuki, S., N. Iwagami, H. Sagawa, M. Ueno, Y. Kasaba, T. Imamura, and E.Nishihara (2008), Imaging spectroscopy of the Venus 1.27-µm, O_2 airglow with ground-based telescopes, Adv. Space Res., 41, 1375-1380.

Piccioni, G., et al. (2008), First detection of hydroxyl in the atmosphere of Venus, Astron. Astrophys., 483, L29–L33, doi:10.1051/0004-6361: 200809761.

Piccioni, G., L. Zasova, A. Migliorini, P. Drossart, A. Shakun, A. García Muñoz, F. P. Mills, and A. Cardesín-Moinelo (2009), Near-IR oxygen nightglow observed by VIRTIS in the Venus upper atmosphere, J. Geophys. Res., 114, E00B38, doi:10.1029/2008JE003133.

Soret, L., J.-C. Gérard, G. Piccioni, and P. Drossart (2010), Venus OH nightglow distribution based on VIRTIS limb observations from Venus Express, Geophys. Res. Lett., 37, L06805, doi:10.1029/2010GL042377.

Soret, L., J.-C. Gérard, G. Piccioni , and P. Drossart (2011), Venus OH Nightglow Distribution from VIRTIS Limb Observations from Venus Express, Geophys. Res. Lett., 37, L06805, doi: 10.1029/2010GL042377.

Svedhem, H., *et al*. (2007), Venus Express - The first European mission to Venus, *Planet. Space Sci*., *55,* 1636-1652, doi:10.1016/j.pss.2007.01.013.

Titov, D.V., *et al.* (2006), Venus Express science planning, *Planet. Space Sci*., *54*, 1279-1297, doi: 10.1016/j.pss.2006.04.017.

Figure captions

Figure 1: Latitudinal distributions of the O_2 1.27-μm and OH limb intensity simultaneously observed with the VIRTIS-M multispectral imager. (a) orbit 733, a1 O_2 airglow, a2 OH airglow(b) orbit 499, (c) orbit 600, and (d) orbit 321. The two emissions show strikingly similar morphology although their relative brightness is variable.

Figure 2: Relationship between the maximum limb intensity of the bright spots observed in the latitudinal distributions of the $O_2(a^1\Delta)$ and OH nightglow emissions (diamonds). The value of the correlation coefficient R is indicated. The trend and the variability of the O_2/OH intensity ratio are similar to those values obtained by Soret et al. (2010) from the full set of individual limb profiles and shown as light grey pluses.

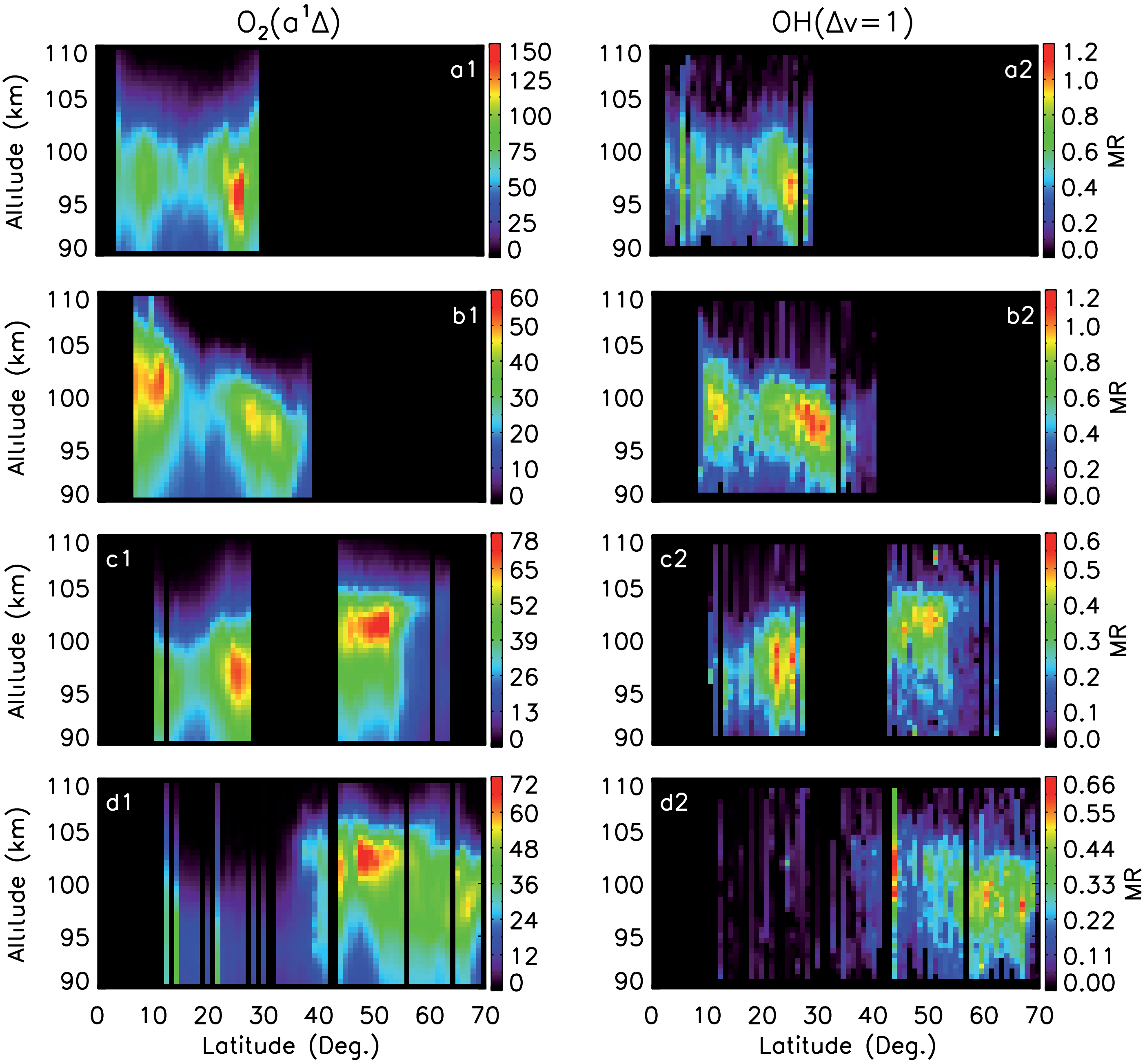
$O_2(a^1\Delta)$
$OH(\Delta v=1)$
a1
a2
b1
b2
c1
c2
d1
d2
Altitude (km)
110
105
100
95
90
150
125
100
75
50
25
0
1.2
1.0
0.8
0.6
0.4
0.2
0.0
MR
60
50
40
30
20
10
0
78
65
52
39
26
13
0
0.6
0.5
0.4
0.3
0.2
0.1
0.0
72
60
48
36
24
12
0
0.66
0.55
0.44
0.33
0.22
0.11
0.00
0 10 20 30 40 50 60 70
Latitude (Deg.)

Figure 1

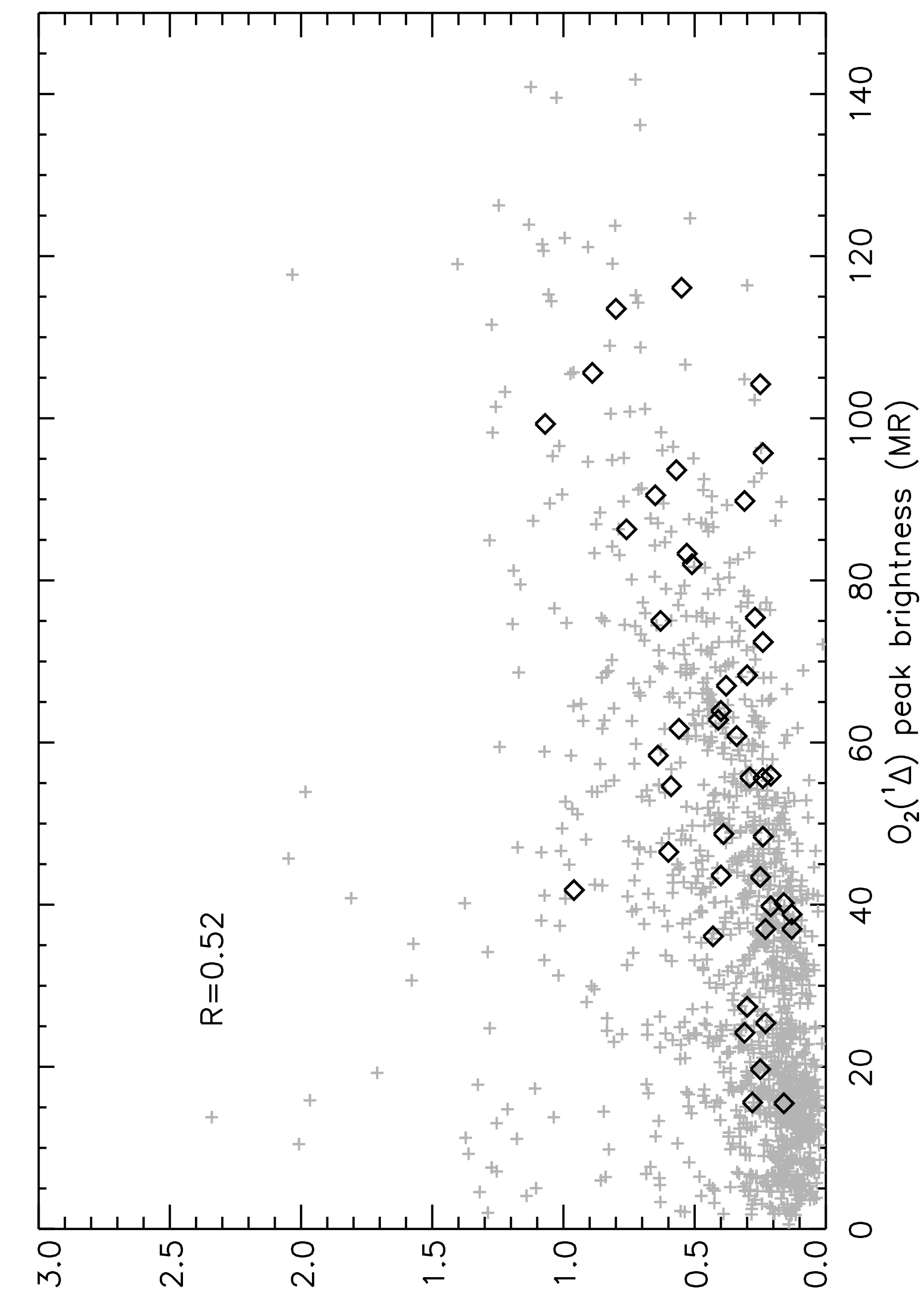
R=0.52
O2(1Δ) peak brightness (MR)
OH* peak brightness (MR)
0
20
40
60
80
100
120
140
0.0
0.5
1.0
1.5
2.0
2.5
3.0

Figure 2